Line broadening and self-absorption of Be IV in a laser-produced plasma*

G. Tondello and E. Jannitti
Centro Gas Ionizzati, Consiglio Nazionale delle Ricerche, Università di Padova, Padova, Italy

A. M. Malvezzi
Centro Informazioni Studi Esperienze, Milano, Italy

(Received 14 October 1974; revised manuscript received 13 September 1976)

The time-integrated spectrum from a plasma of beryllium produced by a 1-GW ruby laser has been observed in the soft-x-ray region with spectral and spatial resolution. The lines of Be IV are broadened near the target. Stark broadening and a Doppler shift due to the expansion of the plasma towards the vacuum combine with the opacity of the plasma itself to give an apparent profile with asymmetrical shift reversal. The equation of radiative transfer is solved in this case with a computed plasma model. Parameters like electron temperature, and density and plasma dimensions have been spectroscopically measured, while Stark parameters have been adopted from the theory. The profiles predicted by the model are in good agreement with the observed ones, especially if time-dependent ionization equilibria are considered. Electron densities inferred from Stark-broadened lines can be estimated up to densities of 10^{21} cm^{-3}.

I. INTRODUCTION

The spectroscopy of laser-produced plasmas has received increasing attention[1,2] both theoretically and experimentally in recent years. This is partially a result, on the one hand, of the diagnostic possibilities of spectroscopy in fusion-oriented experiments (e.g., temperature, density, and expansion-velocity measurements), and, on the other hand, of an intrinsic interest in the properties of the plasma itself. The latter presents quite unique characteristics as a source, for instance, of soft-x-ray radiation[3] suitable for applications like optical pumping of possible lasing media for coherent x-ray generation,[4,5] or production of multicharged ionic species.[6] In addition, there is considerable interest in the investigation of the characteristics of the dense or superdense plasma conditions typical of the interaction of laser beams with the matter.

In all of these studies and applications a quantitative and detailed analysis of the emission and absorption processes taking place in the plasma is most useful. The present paper describes some quantitative time-integrated measurements in the soft-x-ray region and the relevant interpretations in a beryllium laser-produced plasma. The observations were made with spectral and spatial resolution in order to analyze the local distribution of the emission from the plasma. The resonance lines emitted by the Be IV ion appear considerably broadened and asymmetrically self-absorbed, especially near the target. Main factors in explaining the observed broadening have been recognized in the Stark broadening of the levels[7] and in the thermal Doppler broadening. The former effects combine with the Doppler shift due to the strong motion of expansion of the plasma itself. In addition, the optical depth of the plasma, which can be quite high in the center of the resonance lines, considerably alters the locally emitted line profiles.

In order to explain the observations properly and to discriminate among the various effects, a detailed computer model for the plasma has been devised. The model, which is internally consistent, takes into account some phenomenologically determined characteristics of the plasma, like geometrical shape and expansion velocity, and uses as input data spectroscopically derived values for the electron and ion density, temperature, plasma dimensions, and particle velocities. It calculates with the help of a modified transfer equation the emission of the plasma and gives as results the profiles of the resonance lines. The latter compare very satisfactorily both in absolute intensity and in shape with the observations. Discrepancies, when noted, are accounted for quite satisfactorily. Although the final result is arrived at through several steps, it is possible to obtain a unique set of optimized plasma parameters. The Stark-broadening dependence on electron density is observed here up to 10^{21} cm^{-3}, which suggests applications as a diagnostic tool for density determination.

II. EXPERIMENT

The plasma was produced by focusing a Q-switched, 10-J, 10-nsec ruby laser with an aspherical Fresnel lens of 5-cm diameter and 5-cm focal length onto a plane beryllium target in vacuum. The experimental setup, shown in Fig. 1, is

fully described elsewhere.[8] The plasma was observed perpendicular to the direction of the laser beam (the y axis) with a 2-m grazing-incidence spectrograph. A spatial resolution in the y direction ranging between 50 and 150 μm was achieved by inserting in the optical path an additional slit S_2 perpendicular to the entrance slit of the spectrograph. The aperture $A \approx 1/200$ provided a ≈ 100-μm spatial resolution along the x axis, i.e., in the direction of the slit S_2.

The spectra were recorded on Kodak 101-05 plates. From 10 to 40 shots were generally necessary to have properly exposed spectra. The characteristic curve of the plate was determined at the spectral region of interest by measuring the ratio of intensity between the first- and second-order images of various spectral lines.[9] Since the ratio of intensity between the first- and second-order images is a characteristic of a given grating and does not depend on the intensity of the lines, this provided a fixed degree of attenuation between two measurable images. In addition, the intensity ratios between the lines $1s$-$4p$ $L\gamma$, $1s$-$5p$ $L\delta$, and $1s$-$6p$ $L\epsilon$ of Be IV were measured. Since these

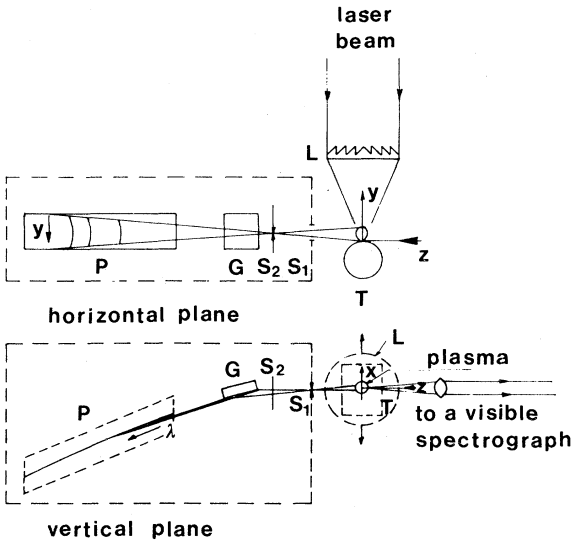

FIG. 1. Schematic of the experimental arrangement in the horizontal and vertical planes. The plasma is formed by focusing a laser beam with aspheric Fresnel lens L onto the target T. The reference axes are as shown. The plasma is observed in the direction of the z axis by a grazing-incidence spectrograph. S_1 is the entrance slit of the spectrograph and is parallel to the y axis. The slit S_2, perpendicular to S_1 and in the direction of the x axis, provides a spatial resolution on the plate P along the y direction. G is the concave grating. The entire focusing assembly can be moved up and down in the vertical plane with respect to the spectrograph as indicated by the two arrows.

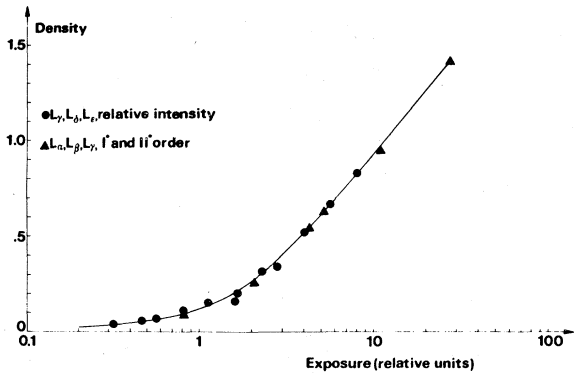

FIG. 2. Characteristic curve, density versus exposure, for Kodak 101-05 plates as used in the present experiment. Circles: attenuation calculated with the relative intensity of the lines $L\gamma$, $L\delta$, and $L\epsilon$ and Be IV; triangles: attenuation provided by the ratio between first- and second-order images of the lines $L\alpha$, $L\beta$, and $L\gamma$ Be IV.

lines, as we will see, are optically thin and moreover their upper levels are in statistical equilibrium at the high-density condition of a laser-produced plasma (at least near the target position), their intensities can be calculated and are proportional to their f numbers. The two methods agree quite well, as can be seen in Fig. 2, where a typical characteristic curve for Kodak 101-05 is reported. Nonreciprocity effects were neglected at these wavelengths.

The grating used in the present experiment was of the same type as the ones absolutely calibrated by Speer[10] and by Irons and Peacock[11] with independent methods in the range 20–120 Å. Allowance has been made for maximum deviations between different replicas of the same master. Hobby and Peacock[9] have also measured sensitivity of Ilford Q-2 plates in the same spectral region in absolute units. Use has been made of these data and a comparison was made between Q-2 and 101-05 plates. The overall accuracy of the absolute calibration is expected to be within a factor of 3. However, use of the absolute calibration proved necessary only for a comparison with the final data provided by the model. All the other measurements have required only relative intensity calibrations. In addition, a spectrograph for the visible and near-uv part of the spectrum observed the plasma in the same direction, but on the other side with respect to the grazing-incidence spectrograph.

III. OBSERVATIONS

The spatially resolved spectrum emitted by the plasma in the region 50–80 Å is shown in Fig. 3.

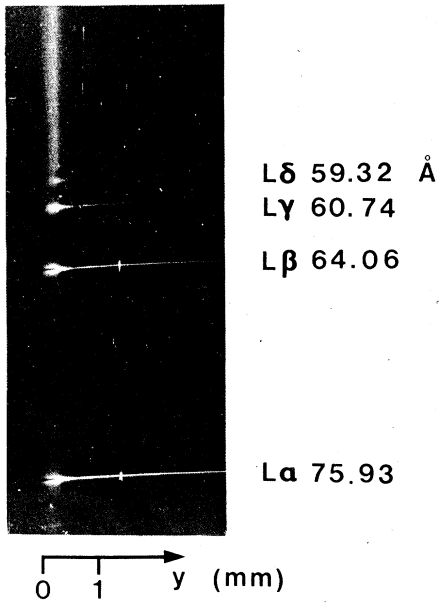

FIG. 3. Space-resolved spectrum emitted by the laser-produced beryllium plasma showing the Lyman series and the recombination continuum. Wavelength scale runs downwards.

The resonance lines $1s$-np, $n=2,\ldots 6$ of the H-like Be IV are seen to be prominent and extend up to a few millimeters from the target position. The lines are followed at shorter wavelengths by the recombination continuum. The lines are clearly broadened near the position of the target, and the apparent broadening decreases away from the target. For the lines $L\alpha$ and $L\beta$ a strong self-absorption near the center of the line is present. However, as can be seen from Fig. 3 and from Figs. 4, 5, and 6, which show a set of intensity profiles derived from the plates for the lines $L\alpha$, $L\beta$, and $L\gamma$ at various distances from the target, the reabsorption peak is not symmetrical, but is shifted towards the shorter wavelengths. This shift is, within the experimental errors of measurements, constant for all distances from the target and also roughly proportional to the wavelength of the lines, $\Delta\lambda \approx 3\times 10^{-2}$ Å for $L\alpha$. Note that the absorption peak, having a constant shift with respect to the emission peak, tends to disappear at large distances from the target where the lines become narrower. The weak continuum present among the lines may originate as a superposition of various contributions, e.g., as a second-order image given by the grating spectrograph of the free-bound continuum around 35 Å, as bremsstrahlung or a free-free continuum emitted by the plasma, or as a recombination continuum of the He-like Be III,

$$\text{Be IV} + e \rightarrow \text{Be III} + h\nu .$$

In the following analysis as well as in Figs. 4–6 this continuum has been subtracted from the line profiles.

The profiles reported in Figs. 4–6 are in absolute units of intensity emitted by the plasma. For the profile corresponding to the position $y = 0.05$ mm from the target, a correction to the intensity has been added to take into account the finite space-resolving power of the spectrograph.

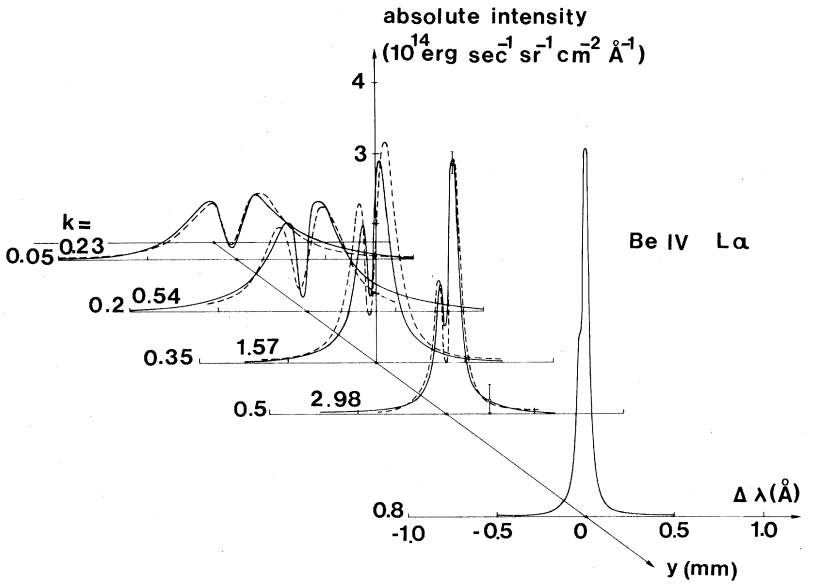

FIG. 4. Profiles for the Be IV $L\alpha$ line at various distances y (in mm) from the target. Dashed curves: computed profiles; solid curves: experimental profiles normalized in intensity, i.e., multiplied by the factors K indicated.

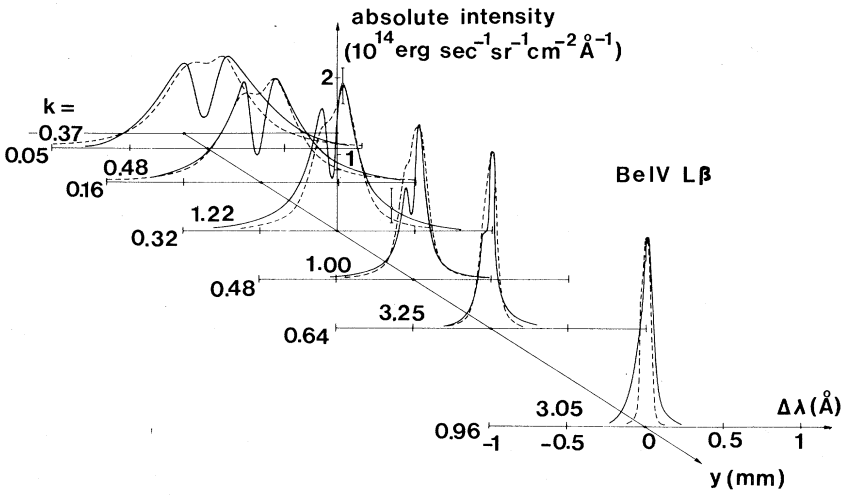

FIG. 5. Same as in Fig. 4, but for $L\beta$.

IV. INTERPRETATION OF THE RESULTS AND A MODEL FOR THE PLASMA

The previously described observations can be interpreted in the following way. With reference to Fig. 7 assume that the y axis is in the direction of the incoming laser beam; $y=0$ is the position of the target. The z axis is in the direction of observation. The plasma volume observed at a point in the focal plane of the spectrograph is centered in the (y,z) plane and extends from $+z_0$ to $-z_0$. The emission of resonance lines like $L\alpha$, $L\beta$, and $L\gamma$ Be IV, comes perferably from the central portion of the plasma,[3] where the more ionized species are contained.[12] The energy levels are broadened due to various local effects like the Stark effect due to the ion and electron microfields[13] and the thermal Doppler effect due to the thermal motion. This broadening, however, decreases with $|z|$, so that the radiation emitted by the core is partially reabsorbed on its way out because of the optical opacity of the plasma mainly in the center of the profile. Moreover, the plasma freely expands[12] from the focal spot towards the vacuum with a velocity v as shown in Fig. 7. The z component of the velocity, v_z, causes a Doppler shift $\Delta\lambda$ towards the blue, constant with y. The obtained value $v_z \approx 1.3\times10^7$ cm/sec is consistent with previous measurements for the same range of laser energies.[3,12]

For computing the emergent line profiles, the transfer equation[14] has been integrated along the line of sight of the spectrograph (i.e., the z direction) for a set of values of y and $\Delta\lambda$. The absorp-

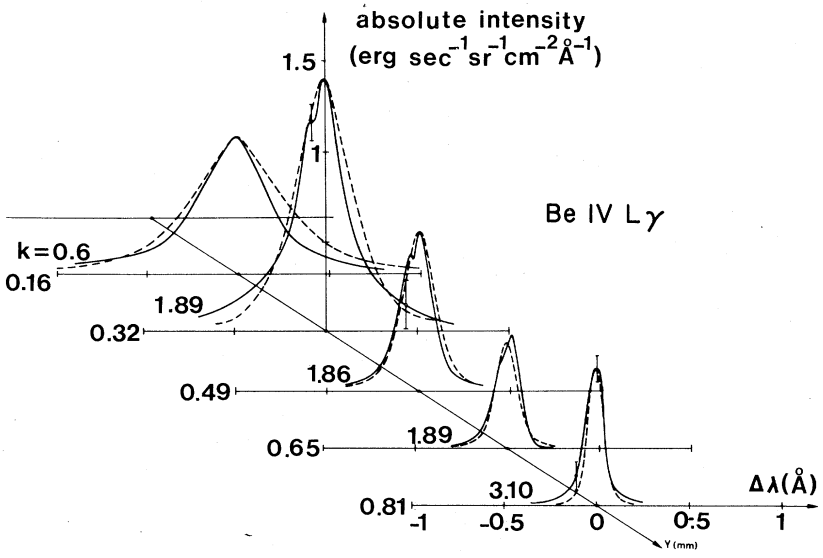

FIG. 6. Same as in Fig. 4, bu for $L\gamma$.

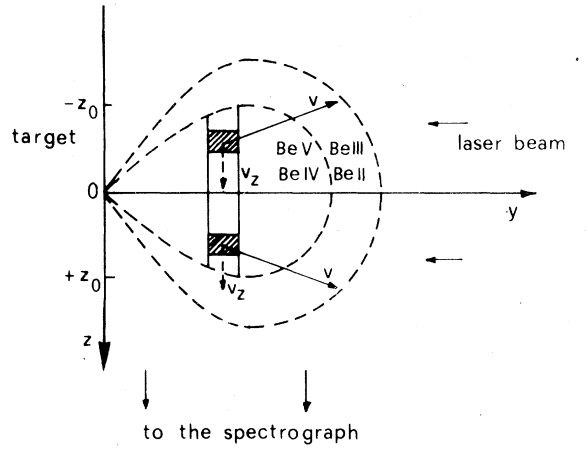

FIG. 7. Geometry of the laser-produced plasma at a given time. The plasma is formed at the surface of the target and is expanding with velocities v towards the vacuum. The x axis is perpendicular to the plane of the drawing, y is in the direction of the incoming laser beam, and z is in the direction of observation. The plasma is assumed to be rotationally symmetric around the y axis, and the ionic species distributed according to the figure, i.e., the more highly ionized species near the center and the less ionized outside; v_z indicates the velocity component in the direction of sight.

tion and emission coefficients (χ and J) of the transfer equation[8] take into account the plasma expansion,[15] the values $n_i(y,z)$ of the populations of the upper ($i=2,3,4$) and lower ($i=1$) levels of the atomic transition, and the local spectral profile $\Phi(\Delta\lambda,y,z)$.[14] The latter, which is normalized in area, accounts for the local broadening processes of the energy levels here considered. For a full description see Ref. 8.

The profile $\phi(\Delta\lambda,y,z)$ is accordingly made up from a convolution between a profile accounting for the Stark broadening and a Gaussian-shaped function due to the thermal Doppler broadening.[14] In order to account for the Doppler shift due to the motion of expansion of the plasma, we have assumed a local shift $\Delta\lambda$ of the center of the profile with respect to the unperturbated wavelength λ_0 corresponding to a free streaming of the plasma with constant absolute velocities and directions distributed on a solid angle with apex at the point $y=0$, $z=0$ and aperture $2z_0/y$; see Fig. 7.

Because of the complexity of the problem, recourse was made to a computer program, which is described in more detail elsewhere.[17] Briefly, the program acquires as input data the Stark profiles, the electron density $n_e(y,z)$, the population densities of the levels of Be IV, $n_i(y,z)$ ($i=1,\ldots,4$), and the ionic temperature T_i. Next the program calculates for various values of z the convolution profile. Subsequently, after the normalization the program computes the Doppler shifts and finally integrates the transfer equation between the boundaries of the plasma, also provided as input data. The final results are the intensity profiles of the lines in absolute units for various values of the distance y from the target.

V. EVALUATION AND MEASUREMENT OF PLASMA PARAMETERS

In order to obtain the intensity profiles for the lines emitted by the plasma, it is necessary to know the local values for the following parameters: (a) the Stark broadening and electron density $n_e(y,z)$; (b) the electron and ion temperatures T_e and T_i, and expansion velocity of the plasma v; (c) the geometrical depth of the plasma, z_0; and (d) the population density distribution among the upper levels ($i=2,3,4$) $n_i(y,z)$ and the ground level $n_1(y,z)$.

The values adopted for these parameters are partly a result of space-averaged and time-integrated measurements, for instance, of electron density and temperature, and partly depend on some *ad hoc* hypothesis adopted, e.g., for the local distribution. In Sec. VII the various assumptions adopted as working hypotheses will be subjected to a critical examination and their influence discussed.

A. Stark broadening and electron density

The Stark broadening has been evaluated using the calculations reported by Griem[16] for the lines $L\alpha$ and $L\beta$ of He II and $L\gamma$ of H I with a Z^{-5} scaling as described in details in Ref. 8.

Typical values of $\Delta\lambda$(HWHM) for an electron density $n_e=10^{20}$ cm^{-3}, $Z_p=4$ (Be nuclei full stripped) are reported in the third column of Table I. For the line $L\gamma$ there is very little difference with respect to a simplified theory previously reported by Griem[18] and adopted for the interpretation of the broadening observed by Malvezzi *et al.*[7] Moreover, as will be shown later, the contribution to

TABLE I. Half widths $\Delta\lambda$ at half maximum for the resonance lines of Be IV due to the Stark broadening ($n_e=10^{20}$ cm^{-3}) and Doppler thermal broadening ($T_e=T_i=80$ eV).

Line	Wavelength (Å)	$\Delta\lambda$ Stark (10^{-2} Å)	$\Delta\lambda$ Doppler (10^{-2} Å)
$L\alpha$	75.93	0.8	0.8
$L\beta$	64.06	12	0.67
$L\gamma$	60.74	23.6	0.64

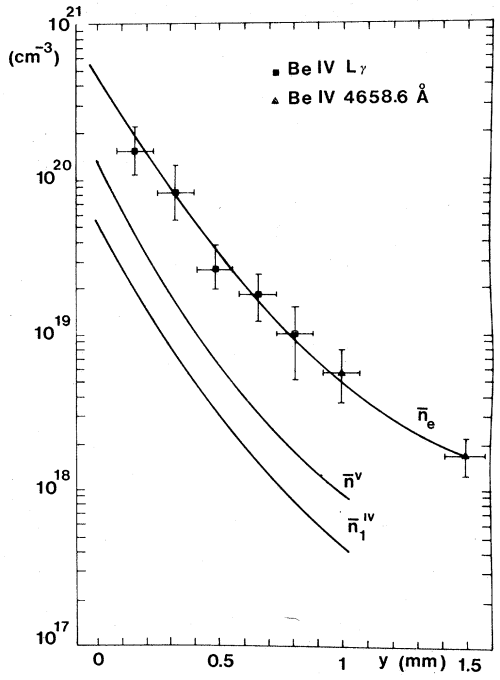

FIG. 8. Electron density and population densities $\bar{n}^V$ of fully stripped Be ions and $\bar{n}_1^{IV}$ of Be IV ions in the ground state, averaged along the line of sight versus y, the distance from the target. The squares correspond to determinations of the Stark broadening of the $L\gamma$ line, the triangles to determinations of the Stark broadening of the line $n=6$ to 5 Be IV (Ref. 6).

the total broadening of the $L\gamma$ line due to the Doppler component and the overall deforming effect due to the opacity turns out to be quite small compared to the Stark broadening, at least for values of the distance from the target $y<0.8$ mm. We shall then retain the values of average electron density $\bar{n}_e(y)$ previously determined[7] with the Stark broadening of the $L\gamma$ line. This is shown in Fig. 8. Note that the values for the electron density are a little lower than the ones previously determined[7] as the average of all the observations $(L\alpha,\beta,\gamma)$.

As far as the dependence of the electron density on the coordinate z is concerned, we have assumed simply a Gaussian behavior, i.e.,

$$n_e(y,z) = f(y)\exp\left[-\left(\frac{z}{z_1}\right)^2\right]$$

$$= \alpha\bar{n}_e(y)\exp\left[-\left(\frac{z}{\beta z_0/\sqrt{\ln 2}}\right)^2\right], \qquad (1)$$

where α is the ratio between the peak value for the electron density and the experimentally measured one and β the ratio between the half-width of the Gaussian profile (1) and the observed plasma dimension.

With the electron density values given by (1), the Stark profiles have been calculated and are reported in detail elsewhere.[17]

B. Electron and ion temperature and expansion velocity of the plasma

The plasma electron temperature T_e as a function of y has been derived by measuring the slope[8] of the recombination continuum.[19] The measurements have been made at several distances y and at wavelengths of ≈ 57 Å (corresponding to the series limits, at 49 Å, before the carbon K jump) and at 35 Å, the last point with measurable intensity. The result is shown in Fig. 9 and is consistent with values found in previous works[3] at comparable laser intensities. Uncertainties both in the spatial coordinate y and in the values of T_e have been plotted. Moreover, we have assumed that the ion and electron temperatures are equal and constant along the z direction. The Doppler thermal broadening assuming $T_i = T_e = 80$ eV is shown in the fourth column of Table I. As can be seen, it is comparable to the Stark broadening only for the $L\alpha$ line, in all other cases being sensibly smaller.

In order to take into account the expansion velocity of the plasma, the maximum Dopper shift

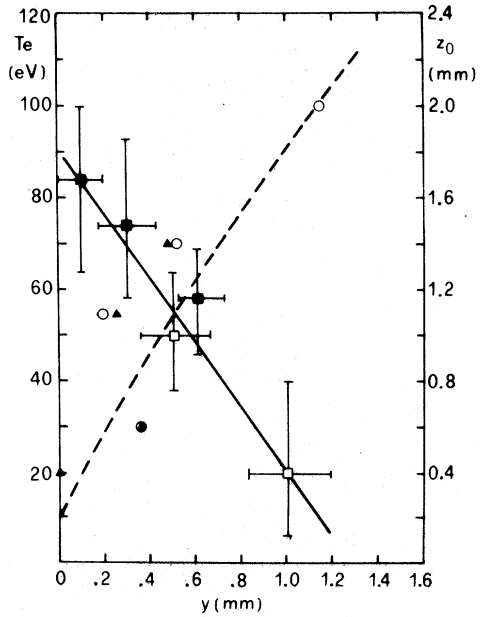

FIG. 9. Electron temperature and plasma half dimension z_0 versus y. Solid squares refer to measurements performed with spatial resolution $\Delta y = 150/\mu$m; open squares, with spatial resolution $\Delta y = 250/\mu$m. Open circles refer to measurements with Be III resonance lines; triangles, to measurements with Be IV resonance lines.

$\Delta\lambda_0$, corresponding to the plasma boundary, has been taken as the input parameter.[8] The optimum value happens to be equal to the wavelength difference between the emission and absorption maxima.

C. Geometrical depth of the plasma

With several spectra of the plasma taken at different positions along the x axis (see Fig. 1), the time-integrated boundaries $z_0(y)$ of the plasma itself have been evaluated. A reference for the central position in the target, corresponding to $x=0$, was provided by superimposing the spectrum of a different material (Al). This method, although more complicated, has been preferred to scanning the plasma itself in visible or near-uv light or to taking images with a converter camera, because there is much less influence from stray light[3]; in the visible region the latter arises more from low stages of ionization and does not necessarily follow the geometry of the dense, hot inner core of the plasma. Figure 9 shows the half dimension z_0 as function of y. Again the results are in agreement with previous observations.[12] The geometrical width of the plasma so obtained is the same in the light of the Lyman lines of Be IV as for the resonance lines $1s^2$-$1snp$ of Be III, but is considerably smaller than the one observed in visible light with the spectrograph indicated in Fig. 1, supporting a model of plasma like that shown in Fig. 7.

D. Distribution of population

For evaluating $n_i^{IV}(y,z)$, $i=1,\ldots,4$, i.e., the population in the various levels of Be IV, it is first necessary to know the distribution of the ions among ionized states and successively the distribution among the various bound states of Be IV. From the neutrality equation one gets

$$n_e = 4n^V + 3n^{IV}, \tag{2}$$

where n^V is the density of fully stripped beryllium ions and n^{IV} is the total density of Be IV ions in all bound states. The contribution from the Be III ions is neglected because in the central region of the plasma, which we are interested in now, it turns out to be quite small.

We have measured the ratio $\bar{n}^V/\bar{n}_i^{IV}$, $i=4$, where the bars stand for values averaged from $-z_0$ and $+z_0$, by measuring the ratio of intensity of one high n-level line of Be IV with respect to a similar line of Be III.

The population of a level of an ion with a value of principal quantum number n large enough can be correlated to the population of the next stage of ionization assuming local thermodynamic equilibrium (LTE) among them by the Saha-Boltzmann equation.[14] The condition for this being true is that the electron density must satisfy[19]

$$n_e > 1.7\times10^{14} T_e^{1/2} X^3(Z,n)\ \text{cm}^{-3}, \tag{3}$$

where X is the ionization potential from level n of the ionic species of charge Z; T_e and X are in eV. We have chosen for the measurement the $L\gamma$ Be IV and $1s^2$-$1s3p$ Be III lines. Equation (3) gives, with the measured values of T_e, $n_e=2\times10^{18}$, easily satisfied by our plasma (see Fig. 8).

The intensity of the $L\gamma$ Be IV line can be expressed as

$$I \propto \frac{\omega_4^{IV}}{\omega_1^V}\frac{A_{4-1}^{IV} h\nu}{(kT_e)^{3/2}}\bar{n}_e\,\bar{n}^V \exp\left(\frac{X(\text{IV},4)}{kT_e}\right) z_0, \tag{4}$$

where ω is the statistical weight of the specified level, A is the transition probability, and the other symbols have already been defined. A similar expression holds for the intensity I' of the $1s^2$-$1s3p$ Be III line, with suitable changes in the parameters.

The ratio of the two intensities gives

$$R = I/I' = 2.8\,\bar{n}^V/\bar{n}_1^{IV}, \tag{5}$$

all other quantities having cancelled or being substituted with the proper numerical values. The intensities of the two lines have been measured by integrating the profiles and assuming them to be sufficiently optically thin that the measurements are not altered appreciably. The latter condition is that the optical depth at line center $\tau_0<0.4$; in this case the total intensity differs by less than 10% from the optically thin value.[14] We will see that this is mostly the case for both the $L\gamma$ Be IV and the $1s^2$-$1s3p$ Be III lines. A correction was inserted when this was not true. In this way the value 2.2 for the ratio $\bar{n}^V/\bar{n}_1^{IV}$ was found at any distance y from the target within ~20%.

Note that, for the validity of the previous measurement, it is necessary that the zone of plasma emitting the Be III and Be IV lines be the same in order for the plasma depth to cancel out. This corresponds to the observations reported above.

It is now necessary to determine the distribution of populations among the bound states of Be IV in order to be able to solve Eqs. (2) and (5). LTE conditions have already been assumed between the Be IV $n=4$ level and the fully stripped nuclei, condition (3) being satisfied. The latter is also fulfilled by levels with $n>4$. As far as the levels $n=3$ and $n=2$ are concerned, it is necessary to note that condition (3) is derived in the optically thin case when the emitted photons can escape freely. As will be shown later, the optical depth for the $L\alpha$ and $L\beta$ lines is not negligible; this has the effect of decreasing the net radiative decay rate of the $n=3$ and $n=2$ levels.[19] Consequently, the criterion (3) can be relaxed, and it is a justified assumption to take also the $n=3$ and $n=2$ levels in

LTE with the fully stripped nuclei.

In Fig. 8 the obtained values for $\bar{n}^{V}$ and $\bar{n}_1^{IV}$ versus y are shown. The population in the excited levels of Be IV turns out to be considerably smaller than the population in the ground level, e.g., $\bar{n}_4^{IV} \approx 3\times10^{15}$ cm^{-3} at $y = 0.4$ mm.

The behavior with z of the populations n_1^{IV} and n^{V} follows immediately from (2) and (1); this corresponds, the temperature T_e being constant with varying z, to choosing an ionization equilibrium independent of the electron density. Since the densities n_i^{IV}, $i \geq 2$, have been determined by the LTE condition, their dependence from z will be steeper, i.e.,

$$n_i^{IV} \propto \exp[-2(z/z_1)^2]. \tag{6}$$

Consequently, the source function[14]

$$S = J/\chi \propto n_i/n_1$$

is not constant with z but has a Gaussian dependence.[15]

VI. COMPARISON BETWEEN THE MODEL AND EXPERIMENTAL RESULTS

Inserting in the calculations the values of the parameters previously discussed, the computed profiles of the Be IV $L\alpha, L\beta, L\gamma$ lines were obtained. They appear as dashed lines in Figs. 4, 5, and 6 respectively. The profiles are given in absolute intensity units and correspond to the following optimal values of the parameters described in Sec. IV:

$$\Delta\lambda_0 = 4\times10^{-2}\ \text{Å}, \quad \alpha = 0.9, \quad \beta = 0.6.$$

The computed profiles are in good agreement with the experimental ones. In particular, the effects on the profile of self-absorption, the asymmetry due to expansion, and the total width for the $L\alpha$ and $L\beta$ lines are correctly predicted by the model. The $L\gamma$ line shows only a very weak self-absorption, and its profile is in practice the integral of the locally emitted profiles along the plasma depth. The peak absolute intensities of the $L\alpha$, $L\beta$, and $L\gamma$ lines derived from the model are in sufficient agreement with the one experimentally determined, taking into account the large uncertainty of the latter. However, there is a difference in the intensity behavior with y between the computed profiles (which are decreasing with y) and the observed profiles, especially for $L\alpha$. In Figs. 4–6, for each pair of profiles we also indicate the normalization factor k, i.e., the ratio between the intensities of the computed and experimental profiles. A possible explanation for this discrepancy will be provided in Sec. VII. All of these results are considered as an overall proof of the validity of the plasma model and the computations.

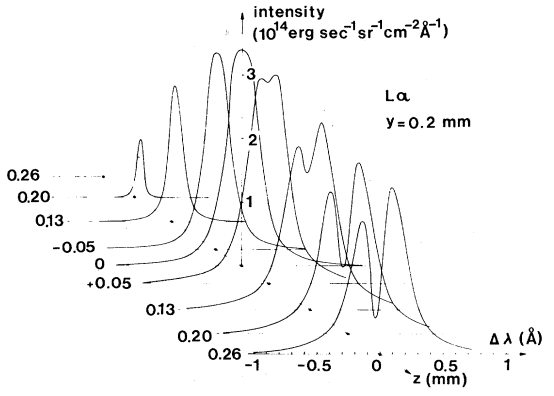

FIG. 10. Effect of the optical depth on the apparent profile. The computed intensity profile of the $L\alpha$ line at $y = 0.2$ mm from the target is plotted at various sections of the plasma corresponding to different values of the coordinate z along the line of sight.

The position of the minimum and the relative position of the two maxima are very sensitive to the $\Delta\lambda_0$ value. The latter, in contrast, has a negligible effect on the total width of the profile. This is, on the contrary, almost completely controlled by the parameters α and β describing the spatial distribution of the densities. By increasing both α and β, the overall self-absorption effect and the total width of the computed profile increase, as is evident from (1). However, by increasing only β, the profile also becomes more symmetric. It is then possible to arrive at a unique set of optimal values for α and β.

In Fig. 10 the computed profile of the $L\alpha$ line at $y = 0.2$ is reported as a function of the geometrical depth z from $-z_0$ to $+z_0$. It can be seen that the resulting profile is a typical opacity-broadened profile, the asymmetric self-absorption increasing the plasma depth.

Another noteworthy observation is the fact that the $L\beta$ computed profile shows a significantly smaller absorption peak than the one observed experimentally. Since all the parameters can be fixed by agreement with the observations for the $L\alpha$ and $L\gamma$ lines, this discrepancy could be assigned to the Stark profile adopted.[16] For complete agreement with the experiment, the Stark broadening for the $n = 3$ level should be somewhat smaller than the one we adopted.

The substitution of a Lorentzian shape for z in Eq. (1) does not produce appreciable difference in the profiles. On the other hand, a hypothesis that is quite sensitive is the dependence of the upper-level populations n_i^{IV}, $i \geq 2$, on z, with a shape given by Eq. (6). In Fig. 11 we show for comparison the $L\alpha$ profile for $y = 0.2$ mm obtained assum-

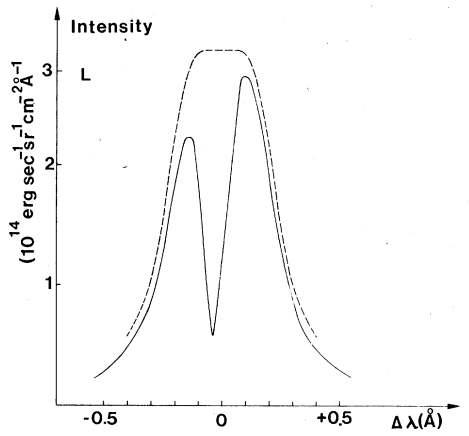

FIG. 11. Computed profiles of the Be IV $L\alpha$ line at $y = 0.22$ mm. The solid curve corresponds to a plot of the upper-state population versus z of the type $n_2^{IV} \propto \exp[-2(z/z_1)^2]$. The dotted curve corresponds to a functional dependence on z of the type $n_2^{IV} \propto \exp[-(z/z_1)^2]$.

ing for n_2^{IV} a dependence on z given by (1) instead of the one given by (6). Clearly, the effect of flattening and total elimination of the absorption dip in the middle of the profile can be seen, in disagreement with the observations. The last hypothesis corresponds indeed to adoption of a source function S independent of z.[15] It follows then that the assumptions leading to formula (6) corresponds to the experimental situation.

In Fig. 12 the optical depth at line center is reported. Some of the leading assumptions of the present work are entirely confirmed, namely, the fact that the $L\gamma$ line is practically always optically thin. In contrast, $L\alpha$ and to a lesser extent $L\beta$ are altered by the opacity effect, which in the former line takes quite high values.

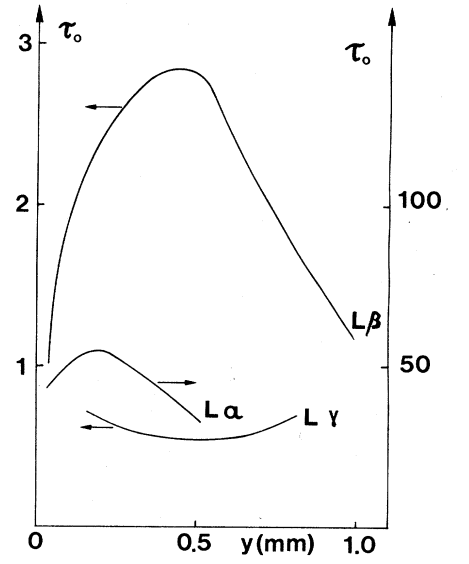

FIG. 12. Computed optical depths τ_0 at line center versus y for the $L\alpha$ line (scale at the right) and the $L\beta$ and $L\gamma$ lines (scale at the left).

VII. DISCUSSION AND CONCLUSIONS

The space-resolved but time-integrated results presented in this paper have been compared with a static model for the plasma. The agreement achieved, taking also into account the low dynamical range of the photographic detectors in the X UV region, seems to indicate that for our experimental conditions, the line spectrum of Be IV is mainly emitted during a quasistationary phase of the plasma evolution. Therefore, the time-averaged but space-resolved values of the various plasma parameters thus inferred can be considered as representative of the plasma itself.

The measured density n_1^{IV} is much higher than that deduced assuming static corona and LTE conditions by factors of 50 and ~500, respectively. This discrepancy could be explained by the fact that in our case a steady-state equilibrium is not reached. In fact, the confinement time necessary for the validity of the steady-state approximation[21] turns out to be too long compared with the time necessary for an ion to travel through the high-density region.[20]

It is then evident that there is not enough time for a complete equilibrium between Be IV and Be V to be established in a laser-produced expanding plasma. An excess of Be IV with respect to the values predicted by both the static LTE and static corona equilibrium models will be found at a given temperature in the laser-produced plasma.[22] This excess will be found mainly in the ground state because the relaxation times connected to the excited levels and related to the transition probabilities A_{i1} to the ground state are quite small; typically, $\tau_{21} \approx 4\times10^{-10}$ sec for Be IV. Some excess of population with respect to the values predicted by the LTE is reasonable also for the excited levels $n = 2, 3, 4$ (in decreasing quantity). Because of the inequality (3) and the decreasing density of the plasma as y increases, it is expected that the difference for the actual case from the LTE equilibrium will be more pronounced moving away from the target. This is entirely confirmed, taking into account the discrepancy previously noted between the absolute intensities of the lines as computed from the models, i.e., assuming perfect LTE equilibrium to hold everywhere, and the measured intensities. It follows that the excess of intensity measured for large values of y with respect to the

intensities computed by the model is indicative of a local excess of population n_i^{IV} with respect to the values predicted by the LTE conditions. The discrepancy, as can be seen from (3), is larger for $L\alpha$ than for $L\beta$ or $L\gamma$ as is, in fact, observed; see Figs. 4–6.

The general agreement between the profiles computed with the model and the experimental profiles demonstrates the validity of both the measurements and the various assumptions included in the model. In particular, the agreement in the shape of the profiles with the asymmetry towards the short wavelengths is a clear indication of the mechanism of the expanding plasma and the absorption for the various elements shifted by the Doppler effect. The $L\gamma$ line, as was originally assumed, is everywhere almost optically thin; the electron density derived from the Stark broadening of the latter has been shown to be consistent with the various observations. It appears possible to use the Stark broadening of the $L\gamma$ line in a laser-produced plasma for evaluating electron density up to 10^{21} cm^{-3}.

---

*Work partially performed under CNR/CISE Contract No. 7400831.11.

[1]D. Colombant and G. F. Tonon, J. Appl. Phys. 44, 3524 (1973).
[2]F. E. Irons and N. J. Peacock, J. Phys. B 7, 2084 (1974).
[3]B. C. Boland, F.E. Irons, and R. W. P. McWhirter, J. Phys. B 1, 1180 (1968).
[4]B. A. Norton and N. J. Peacock, J. Phys. B 8, 989 (1974).
[5]F. T. Arecchi, G. P. Banfi, and A. M. Malvezzi, Opt. Commun. 10, 214 (1974).
[6]N.J . Peacock and R. S. Pease, J. Phys. D 2, 1705 (1969).
[7]A. M. Malvezzi, E. Jannitti, and G. Tondello, Opt. Commun. 13, 307 (1975).
[8]E. Jannitti, P. Nicolosi, G. Tondello, L. Garifo, and A. M. Malvezzi, in *Laser Interaction and Related Plasma Phenomena*, edited by H. S. Scharz and H. Hora (Academic, New York, 1977).
[9]M. G. Hobby and N. J. Peacock, J. Phys. E 6, 854 (1973).
[10]R. J. Speer, J. Spectrosc. Soc. (Jpn.) 23, Suppl. 1, 53 (1974).
[11]F. E. Irons and N. J. Peacock, J. Phys. E 6, 854 (1973).
[12]F. E. Irons, R. W. P. McWhirter, and N. J. Peacock, J. Phys. B 5, 1975 (1972).
[13]F. E. Irons, J. Phys. B 6, 1562 (1973).
[14]J. Cooper, Rep. Prog. Phys. 29, 35 (1966).
[15]F. E Irons, J. Phys. B 8, 3044 (1974).
[16]H. R. Griem, *Spectral Line Broadening by Plasmas* (Academic, New York, 1974).
[17]A. M. Malvezzi, Rapporto CISE, 1977 (unpublished).
[18]H. R. Griem, Astrophys. J. 132, 883 (1960).
[19]R. W. P. McWhirter, in *Plasma Diagnostic Techniques*, edited by R. H. Huddlestone and S. L. Leonard (Academic, New York, 1965), p. 201.
[20]M. Galanti and N. J. Peacock, J. Phys. B 8, 2427 (1975).
[21]E. Jannitti, A. M. Malvezzi, and G. Tondello, J. Appl. Phys. 46, 3096 (1975).
[22]R. W. P. McWhirter, Culham Report No. CLM 150, 1967 (unpublished).

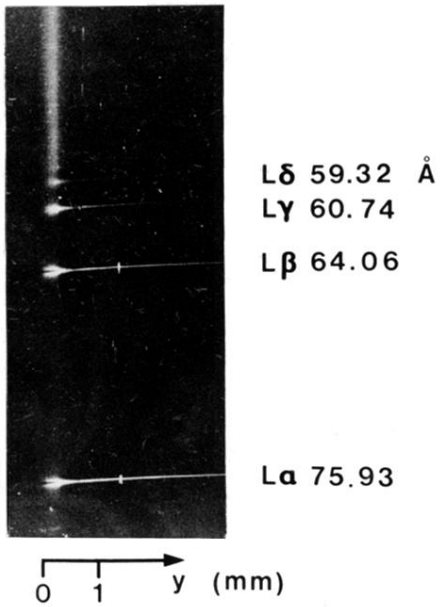

FIG. 3. Space-resolved spectrum emitted by the laser-produced beryllium plasma showing the Lyman series and the recombination continuum. Wavelength scale runs downwards.